Journal of Computational Acoustics, Vol. 5, No. 1 (1997) 117–136

ON TRANSIENT THREE-DIMENSIONAL ABSORBING BOUNDARY CONDITIONS FOR THE MODELING OF ACOUSTIC SCATTERING FROM NEAR-SURFACE OBSTACLES

LOUKAS F. KALLIVOKAS, AGGELOS TSIKAS and JACOBO BIELAK
Computational Mechanics Laboratory, Department of Civil and Environmental Engineering, Carnegie Mellon University, Pittsburgh, Pennsylvania 15213

Received 5 December 1996
Revised 20 December 1996
Accepted 25 December 1996

We have recently developed absorbing boundary conditions for the three-dimensional scalar wave equation in full-space. Their applicability has been extended to half-space scattering problems where the scatterer is located near a pressure-free surface. A variational scheme was also proposed for coupling the structural acoustics equations with the absorbing boundary conditions. It was shown that the application of a Galerkin method on the variational form results in an attractive finite element scheme that, in a natural way, gives rise to a surface-only absorbing boundary element on the truncation boundary. The element — the finite element embodiment of a second-order absorbing boundary condition — is completely characterized by a pair of symmetric, frequency-independent damping and stiffness matrices, and is equally applicable to the transient and harmonic steady-state regimes. Previously, we had applied the methodology to problems involving scatterers of arbitrary geometry. In this paper, we validate our approach by comparing numerical results for rigid spherical scatterers submerged in a half-space, against a recently developed analytic solution.

1. Introduction

A primary difficulty associated with the numerical modeling of exterior wave propagation problems stems from the need to satisfy a boundary condition at infinity. In structural acoustics, i.e. in problems that, over the unbounded exterior region, are governed by the scalar wave equation (transient regime) or Helmholtz's equation (steady-state regime), the pertinent radiation condition is that of Sommerfeld.[1] The success of the many different techniques developed for tackling the exterior structural acoustics problem hinges, in essence, on their ability to accurately model this radiation condition (at infinity, or closer, in some other form). Comprehensive reviews of the various methodologies can be found in Refs. 2–6 amongst others. These methods can be generally classified into one of two types: (a) those based on boundary integral representations, which allow one to completely eliminate the exterior region at the expense of non-locality, and (b) those that truncate the infinite region by introducing an artificial boundary on which one specifies some conditions (absorbing, non-reflecting, etc.) to preclude the occurrence of spurious reflections.

Boundary integral methods and their variants have long been dominant for problems in the frequency domain, as the satisfaction of the radiation condition is guaranteed *a priori* through the use of the Green's functions employed in the formulation. However, and despite the much celebrated dimensionality reduction associated with boundary integral approaches, the resulting dense matrices render three-dimensional applications computationally very expensive (if not infeasible at high frequencies, given present means). A detailed cost comparison of boundary element against finite element methods for frequency-domain problems can be found in Ref. 7; it clearly places the computational advantage in favor of finite elements for both interior and exterior problems. Attempts to reduce the computational cost entailed by boundary integral methods via approaches resulting in block dense matrices have also been reported. For example, the hybrid method presented in Refs. 8–9 uses a boundary integral method in conjunction with domain decomposition and the idea of mapped elements. However, numerical results have, thus far, been reported only for two-dimensional problems. The computational ramifications of the non-local character of the boundary integral methods are exacerbated in the transient regime. While a boundary integral formulation is straightforward in the time-domain in terms of retarded potentials,[10–13] the resulting numerical scheme is non-local in both time and space, and thus computationally unattractive.

By contrast, a domain-based method, such as finite differences or, more commonly, finite elements, might be more desirable for discretizing the continuous problem, for the discretization will result in sparse matrices. But then, there arises a need for a finite computational domain which, in turn, forces the prescription of a condition, typically termed as absorbing, artificial, etc., on the truncation boundary in order to ensure a well-posed problem. There is an exact condition on that truncation boundary,[14] usually referred to as the DtN (Dirichlet-to-Neumann) map,[15–17] which is however non-local in time and space and is similar to a boundary integral representation. Even if the spatial non-locality might be computationally-acceptable for the steady-state problem, the cost associated with the implementation of the condition in the transient regime still necessitates some form of a local approximation of the DtN map (see also Ref. 18). The construction of such local approximants — the absorbing boundary conditions — has been the subject of much research, starting with the pioneering and systematic work of Engquist and Majda.[19,20] They approximated the irrational dispersion relation by rational Padé approximations, thus obtaining a sequence of absorbing boundary conditions in two dimensions. Later, Bayliss and Turkel[21,22] also obtained a family of absorbing boundary conditions through asymptotic expansions of the radial distance for circular and spherical geometries. Various implementations of their conditions in both the time- and frequency-domain within the context of finite elements have also appeared,[23] usually resulting in unsymmetric formulations[24–27] for full-space problems.

It is worth noting that it is difficult for the local approximants to the non-local DtN to be well-behaved at both ends of the frequency spectrum; by construction, many among them are well-behaved at the high-frequency end. Alternatives to absorbing boundary conditions, which are exact at both the low- and high-frequency limits and local in time, are the

well-known doubly asymptotic approximations (DAAs).[28,29] The price one pays for this benefit is having to deal with a spatially non-local boundary, since, at each instant, DAAs couple the response at each point of the artificial boundary with that at every other point.

We remark that within the context of domain-based methods, and in particular of the finite element method, devising absorbing boundary conditions at the continuous level and later coupling them with the domain discretization scheme of choice (e.g. finite elements) is only one of possible paths for tackling the appropriate treatment of the radiation condition (see, for example, Ref. 30 where special elements were devised in order to couple truncated DtN conditions with finite elements). An alternative approach is realized via mapped infinite elements, an idea pioneered by Zienkiewicz and Bettess.[31] In this approach, decay functions that describe the asymptotic behavior of the exact solutions are used at the truncation boundary and special elements, appropriately called infinite, are devised on which the decay functions are mapped.[32,33] The advantage of the infinite elements is their natural coupling to the interior finite elements. One of their disadvantages is that they are derived based on ad-hoc processes that do not necessarily guarantee convergence in all cases; but by far, their primary drawback is that they are limited to frequency-domain formulations. Burnett[34] has recently developed an infinite element based on a prolate spheroidal multipole expansion alleviating many of the shortcomings of past developments. It too, however, cannot be used in the time-domain.

An interesting variant, or enhancement, of the infinite element approach is provided by the so-called wave envelope elements.[35,36] While in standard Galerkin infinite element formulations one uses identical test and trial functions, in the wave element variant the two functions are the complex conjugates of each other. This allows for the ready Fourier inversion of the resulting discrete equations from the frequency- to the time-domain; the resulting semi-discretized form is second-order in time. The development of the wave envelope elements is also predicated on ad-hoc considerations and the resulting formulation is unsymmetric. Nevertheless, they are attractive as they can be equally applied to both steady-state and transient problems — an exception to the rule. The latter is also true of the elements developed herein.

In this paper, we too adopt the idea of absorbing boundaries and favor finite elements for the discretization. Earlier work[37–40] has resulted in a sequence of local approximants to the non-local condition valid for general geometries (smooth) in a full-space. Here we show via the method of images how their use can result in symmetric formulations for half-space problems in either the steady-state or transient regimes. Specifically, we consider a three-dimensional rigid structure submerged in an acoustic fluid at a near-surface location; the free surface is assumed to be a horizontal plane [Fig. 1(a)] (extensions to elastic structures are straightforward and have been included elsewhere[41]). We introduce an artificial boundary of general convex shape [Fig. 1(b)] and prescribe on it a second-order, three-dimensional absorbing boundary condition. We seek to determine the pressure distribution in the fluid within the finite volume bounded by the free surface and the artificial boundary [Fig. 1(b)] given an incident wave impinging upon the structure. We show that the application of a Galerkin process on the variational form gives rise to a simple surface-only absorbing

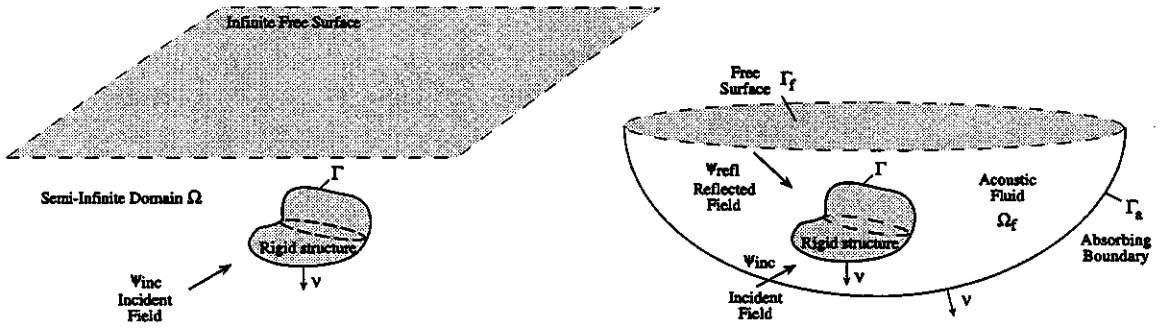

Fig. 1. (a) Model of fluid-structure interaction problem in a semi-infinite acoustic medium Ω bounded by a planar free surface of infinite extent; and (b) reduced model with finite fluid region Ω_f and artificial boundary Γ_a.

boundary element. We validate the method by comparing numerical results for a rigid spherical scatterer against analytical solutions[42] for the case of an obliquely-incident plane wave.

2. The Continuous Problem

2.1. *Variational formulation*

Let us first consider the following problem in full-space; the formulation for the half-space case follows. The development herein parallels earlier work in two and three dimensions.[37–40] Let Γ be a closed surface with exterior $\Omega \subset \Re^3$; Ω is occupied by a compressible, inviscid, linear and homogeneous fluid. We consider the scattering problem in which a traveling plane wave ψ^0 impinges upon a rigid structure [Fig. 2(a)], and seek to determine the scattered (or total) pressure field in Ω. Let us state the strong form of the problem: Given $\psi^0(\mathbf{x}, t)$ with $\mathbf{x} \in \Omega$ find $\psi(\mathbf{x}, t)$ such that

$$\ddot{\psi}(\mathbf{x}, t) = c^2 \Delta \psi(\mathbf{x}, t), \quad \mathbf{x} \in \Omega, \quad t \geq 0, \tag{2.1}$$

$$\psi_\nu(\mathbf{x}, t) + \psi^0_\nu(\mathbf{x}, t) = 0, \quad \mathbf{x} \in \Gamma, \quad t > 0, \tag{2.2}$$

$$\lim_{r \to \infty} r \left(\psi_r + \frac{1}{c} \dot{\psi} \right) = 0, \tag{2.3}$$

$$\psi(\mathbf{x}, 0) = 0, \quad \dot{\psi}(\mathbf{x}, 0) = 0, \quad \mathbf{x} \in \bar{\Omega}. \tag{2.4}$$

In these equations, ψ denotes scattered pressure; $\mathbf{x}$ is the position vector; t is time; ν is the outward unit normal on Γ; c is the velocity of wave propagation; Δ is the Laplace operator, an overdot denotes derivative with respect to time; and ψ_ν denotes the normal derivative of the scattered pressure ψ. Condition (2.3), in which r is radial distance and ψ_r the derivative of the pressure along the radial direction, is the Sommerfeld radiation condition. As indicated by (2.4), the system is taken to be initially at rest.

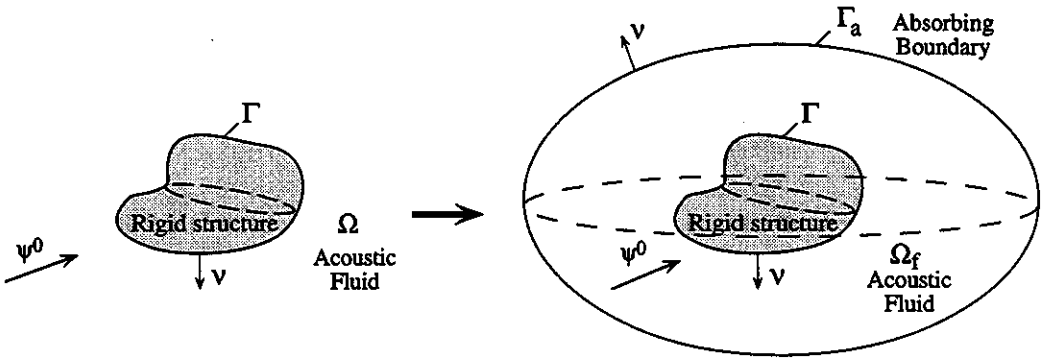

Fig. 2. (a) Model of fluid-structure interaction problem in an infinite acoustic medium Ω; and (b) reduced model with finite fluid region Ω_f and artificial boundary Γ_a.

Next, we truncate the unbounded region Ω by introducing an artificial boundary Γ_a that contains Γ in its interior; this gives rise to the bounded sub-domain Ω_f, as shown in Fig. 2(b). Then, in order for the solution ψ to coincide with that of the original problem (the one defined over Ω) within the truncated region Ω_f, it is necessary to specify a boundary condition on Γ_a that, at a minimum, will ensure that the outgoing waves crossing Γ_a are undisturbed by its presence. This boundary condition, which can be determined in terms of the actual solution ψ on Γ_a is of the form

$$\psi_\nu(\mathbf{x}, t) = \mathcal{F}[\psi^t(\cdot,\cdot)](\mathbf{x}), \quad \mathbf{x} \in \Gamma_a, \tag{2.5}$$

in which the dots following ψ^t indicate dummy variables, and $\mathcal{F}$ is an integral operator that depends on ψ^t; and ψ^t denotes the time history of ψ, i.e.

$$\psi^t(t) = \psi(t-\tau), \ \forall\tau : 0 \le \tau \le t. \tag{2.6}$$

$\mathcal{F}$ is non-local in time and space, that is to say, the motion at any given instant t at every point on the artificial boundary Γ_a is coupled with the time histories of all other points on Γ_a. The non-local character of the exact $\mathcal{F}$ makes it unsuitable for implementation in the context of the finite element method. Herein, as shown later, we employ a localized approximant of $\mathcal{F}$ — a second-order absorbing boundary condition — that is particularly suitable for numerical implementation using finite elements.

With the introduction of the artificial boundary Γ_a and the boundary condition (2.5), one can write a strong statement for the truncated domain Ω_f analogous to (2.1)–(2.4). The variational form of that statement can be easily shown to be

$$\frac{1}{c^2}\int_{\Omega_f} \delta\psi\,\ddot{\psi}\,d\Omega_f + \int_{\Omega_f} \nabla\delta\psi\cdot\nabla\psi\,d\Omega_f - \int_{\Gamma_a} \delta\psi\,\psi_\nu\,d\Gamma_a = \int_\Gamma \delta\psi\,\psi^0_\nu\,d\Gamma. \tag{2.7}$$

Equation (2.7) must hold true for arbitrary $\delta\psi$. It is important to observe that, upon spatial discretization, (2.7) will lead to a symmetric system of ordinary differential equations provided one can ensure the symmetry of the term in (2.7) containing ψ_ν. If one were to substitute the exact condition (2.5) for ψ_ν in (2.7), a highly non-local formulation in both time and space would result. We seek to reduce the non-locality by suitable approximants. Our process for obtaining the localized approximants gives rise to a family of absorbing boundary conditions; some details are provided in the next section. Notice also from (2.7) that in order to maintain the symmetry of the resulting formulation, one need also cast the approximants in a symmetric form. As it was shown elsewhere,[37–40] the latter is achievable through a decomposition scheme local to the boundary.

2.2. *The absorbing boundary*

A systematic procedure for constructing local approximants to the non-local operator of (2.5) of increasing order and complexity, and for arbitrary convex artificial boundaries in three dimensions has been presented elsewhere.[37–40] Here, we repeat the steps that are essential for the remainder. To this end, let Γ_a be smooth and convex and let it be described by the parametric representation $\mathbf{X}(u, w)$, where $\mathbf{X}$ denotes the position vector on Γ_a, and u, and w are the surface parameters (Fig. 3). Then, the second-order absorbing boundary condition is given by[37–40]:

$$\dot{\psi}_\nu + \gamma\,\psi_\nu = -\frac{1}{c}\ddot{\psi} + \left(H - \frac{\gamma}{c}\right)\dot{\psi} + H\,\gamma\,\psi + \frac{c}{2}\left\{\frac{1}{\sqrt{h}}\left\{\left[\frac{1}{\sqrt{h}}(h_{22}\,\psi_u - h_{12}\,\psi_w)\right]_u + \left(\frac{1}{\sqrt{h}}(-h_{12}\,\psi_u + h_{11}\,\psi_w)\right)_w\right] + (H^2 - K)\psi\right\}, \tag{2.8}$$

where γ is an arbitrary non-negative parameter, H and K are the mean and Gaussian curvatures of Γ_a, respectively, and h_{ij} are the components of the Euclidean metric tensor

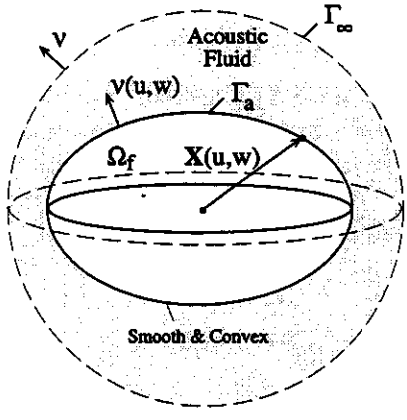

Fig. 3. Surface parameterization of artificial boundary Γ_a.

on Γ_a, i.e.

$$h_{11} = E \equiv \mathbf{X}_u \cdot \mathbf{X}_u \,, \tag{2.9}$$

$$h_{12} = h_{21} = F \equiv \mathbf{X}_u \cdot \mathbf{X}_w \,, \tag{2.10}$$

$$h_{22} = G \equiv \mathbf{X}_w \cdot \mathbf{X}_w \,, \tag{2.11}$$

$$h = EG - F^2 \,. \tag{2.12}$$

The constant γ above has been introduced for stability. In Refs. 38 and 40 we derived (2.8) by using asymptotic expansions in the Laplace transform domain of the solution to the problem exterior to Γ_a. The parameter γ is introduced into these expansions to ensure the stability of the solution when the expansions are transformed back to the time-domain. From a physical point of view, γ represents a certain amount of damping introduced through the boundary Γ_a. Its value should be greater than, or equal to, a critical value γ_{cr} for the particular case of a spherical absorbing boundary[40] $\gamma_{cr} = 0$.

From Eq. (2.8), it is obvious that the second-order absorbing boundary condition cannot be readily incorporated into the variational statement (2.7) as it contains both the normal derivative of ψ, ψ_ν, as well as its first time derivative, i.e. $\dot{\psi}_\nu$. To do this efficiently, we introduce two auxiliary variables on the artificial boundary, $q^{(1)}$ and $q^{(2)}$, and decompose (2.8) into the following set of three equations:

$$-\psi_\nu = \frac{1}{c}\dot{\psi} - H\,\psi - \frac{c}{2\gamma}\mathcal{J}q^{(1)} - \frac{c}{2\gamma}(H^2 - K)q^{(2)} \,, \tag{2.13}$$

$$\mathcal{J}\psi - \mathcal{J}q^{(1)} - \frac{1}{\gamma}\mathcal{J}\dot{q}^{(1)} = 0 \,, \tag{2.14}$$

and

$$\psi - q^{(2)} - \frac{1}{\gamma}\dot{q}^{(2)} = 0 \,, \tag{2.15}$$

where $\mathcal{J}$ is a differential operator defined by

$$\mathcal{J}\cdot = \frac{1}{\sqrt{h}}\left\{\left[\frac{1}{\sqrt{h}}(h_{22}(\cdot)_u - h_{12}(\cdot)_w)\right]_u + \left[\frac{1}{\sqrt{h}}(-h_{12}(\cdot)_u + h_{11}(\cdot)_w)\right]_w\right\} . \tag{2.16}$$

Next, in order to incorporate (2.13)–(2.15) into the variational statement (2.7), we multiply (2.13) by $\delta\psi$; (2.14) by $\delta q^{(1)}$; and (2.15) by $\delta q^{(2)}$, where $\delta q^{(1)}$ and $\delta q^{(2)}$ are appropriate test functions, and integrate the resulting equations over Γ_a. After integrating by parts the terms containing tangential derivatives, there results the following enhanced form

of (2.7):

$$\frac{1}{c^2}\int_{\Omega_f}\delta\psi\,\ddot{\psi}\,d\Omega_f+\int_{\Omega_f}\nabla\delta\psi\cdot\nabla\psi\,d\Omega_f+\frac{1}{c}\int_{\Gamma_a}\delta\psi\,\dot{\psi}\,d\Gamma_a-\int_{\Gamma_a}H\,\delta\psi\,\psi\,d\Gamma_a$$
$$+\frac{c}{2\gamma}\int_{\Gamma_a}\nabla^s\delta\psi\cdot\nabla^s q^{(1)}d\Gamma_a-\frac{c}{2\gamma}\int_{\Gamma_a}(H^2-K)\delta\psi\,q^{(2)}d\Gamma_a$$
$$+\frac{c}{2\gamma}\int_{\Gamma_a}\nabla^s\delta q^{(1)}\cdot\nabla^s\psi\,d\Gamma_a-\frac{c}{2\gamma}\int_{\Gamma_a}\nabla^s\delta q^{(1)}\cdot\nabla^s q^{(1)}d\Gamma_a$$
$$-\frac{c}{2\gamma^2}\int_{\Gamma_a}\nabla^s\delta q^{(1)}\cdot\nabla^s\dot{q}^{(1)}d\Gamma_a-\frac{c}{2\gamma}\int_{\Gamma_a}(H^2-K)\delta q^{(2)}\psi\,d\Gamma_a$$
$$+\frac{c}{2\gamma}\int_{\Gamma_a}(H^2-K)\delta q^{(2)}q^{(2)}d\Gamma_a+\frac{c}{2\gamma^2}\int_{\Gamma_a}(H^2-K)\delta q^{(2)}\dot{q}^{(2)}d\Gamma_a$$
$$=\int_{\Gamma}\delta\psi\,\psi^0_\nu\,d\Gamma\,, \tag{2.17}$$

in which ∇^s is the surface gradient. In addition, $q^{(1)}$, $q^{(2)}$, $\dot{q}^{(1)}$ and $\dot{q}^{(2)}$ are required to vanish at $t=0$. It is noteworthy that (2.17) will lead, upon spatial discretization, to a symmetric system of ordinary differential equations. In other words, the contributions from the absorbing boundary maintain both the symmetric structure of the interior problem and the sparsity of the associated system matrices. Clearly, the decomposition process (2.13)–(2.15) results in the tripling of the degrees-of-freedom on the absorbing boundary Γ_a. However, the benefits derived by the decomposition in terms of accuracy, economy and ease of use outweigh by far the computational cost entailed by the introduction of the additional degrees-of-freedom on Γ_a.

2.3. *Propagation in a half-space*

We consider next the scattering problem that arises when a traveling wave impinges upon a submerged near-surface obstacle (Fig. 1). Typically, in full-space problems, one need only be concerned with the motion within the finite fluid domain; it is expected that the artificial boundary will resolve any outgoing motion to the degree allowed by the order of the approximant (second-order here) to the exact condition on the truncation boundary. By contrast, in half-space scattering problems where full-space absorbing boundary conditions are used, the introduction of an artificial boundary might give rise to additional errors, particularly in regions close to the intersection of the artificial boundary with the free surface. This is especially true if one were to solve for the scattered wavefield in a manner identical to that of the preceding section (the scattered wavefield on the free surface is non-zero). The peculiarity of the half-space problem stems from the presence of a free surface which the absorbing boundary conditions, developed originally for full-space problems, do not readily account for.

To overcome the difficulties imposed by the use of full-space conditions in half-space problems, we resort to the method of images in order to (a) ensure the appropriateness of

the use of full-space conditions such as (2.8), and (b) ensure that the wavefield one needs to solve for remains at zero at all times on the free surface; the use of the method of images will also ensure that the wavefield on the semi-infinite portion of the free surface (exterior to Γ_f) that is excluded from the computational domain, is zero. To this end, we consider the half-space problem depicted in Fig. 1(b) and its adjoint full-space problem depicted in Fig. 4. In Fig. 4, ψ_{refl} represents the image source of the incident pressure field ψ_{inc} in the positive half-plane ($z > 0$). We remark that we require the free surface to be a plane of symmetry of the convex hull bounded by the artificial boundary Γ_a (as in Fig. 4).

Let us define the image source pressure field as

$$\psi_{\text{refl}}(x, y, z, t) = -\psi_{\text{inc}}(x, y, -z, t), \quad \forall z. \tag{2.18}$$

On account of symmetry, the total pressure field is

$$\psi_{\text{tot}}(x, y, z, t) = -\psi_{\text{tot}}(x, y, -z, t), \quad z \geq 0, \tag{2.19}$$

and therefore, on the free surface ($z = 0$), one has

$$\psi_{\text{tot}}(x, y, 0, t) = 0, \tag{2.20}$$

and

$$\psi_{\text{refl}}(x, y, 0, t) + \psi_{\text{inc}}(x, y, 0, t) = 0. \tag{2.21}$$

Let us further define

$$\psi_{\text{tot}}(x, y, z, t) = \psi^0(x, y, z, t) + \psi(x, y, z, t), \quad \forall z, \tag{2.22}$$

where

$$\psi^0(x, y, z, t) = \psi_{\text{inc}}(x, y, z, t) + \psi_{\text{refl}}(x, y, z, t), \quad \forall z. \tag{2.23}$$

ψ in (2.22) denotes a scattered pressure wavefield; in physical terms, ψ is equal to the sum of the scattered fields generated by the real and image scatterers when they are insonified

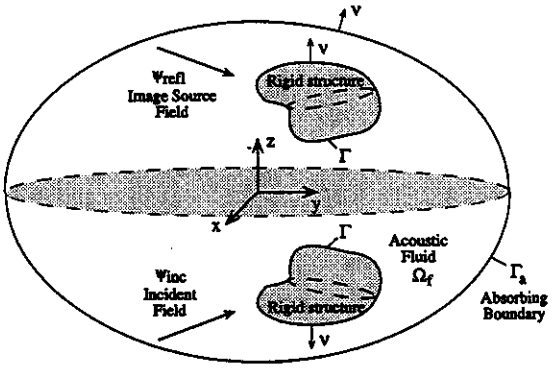

Fig. 4. Full-space problem adjoint to the half-space problem shown in Fig. 1(b).

by ψ_{inc} and ψ_{refl}, respectively. With these definitions, ψ is equal to the part of the scattered field understood as the total wavefield less the free-field wave ψ^0.

Notice that by virtue of (2.18), (2.20), (2.22) and (2.23), there holds

$$\psi(x, y, 0, t) = 0. \tag{2.24}$$

It can be easily seen now that the adjoint problems (Fig. 1(b) and Fig. 4) are equivalent, provided that in the half-space case one solves for the scattered wavefield ψ, prescribes (2.24) on the free surface, and uses ψ^0 (2.23) as the excitation. We remark that ψ_{refl}, as defined in (2.18), represents the free-field reflected wavefield, or in other words, the pressure field that would have been generated in the half-space in the absence of the scatterer. These observations, together with the fact that the right-hand side of the absorbing boundary condition (2.8) is an odd function with respect to the z coordinate, allow for the ready use of the full-space condition (2.8) in the half-space problem without any modification, i.e. one needs to pose the problem for ψ only over the lower half-space in Fig. 1, while prescribing (2.8) on the restriction of the artificial boundary on this half-space. Then, a variational statement similar to (2.17), yet written for a half-space (i.e. Ω_f and Γ_a need to be replaced in (2.17) by their corresponding restrictions on the half-space, $\hat{\Omega}_f$ and $\hat{\Gamma}_a$, respectively), can be readily used to yield solutions for the scattered field ψ.

3. The Discrete Problem

3.1. *Finite elements*

The semi-discretized equations corresponding to the variational form (2.17) can be obtained readily by using standard piecewise polynomials to represent the test and trial functions in (2.17). Details of the procedure can be found in Ref. 37 for the similar two-dimensional case. The resulting ordinary differential equations have the following structure:

$$\mathbf{M}\ddot{\mathbf{U}} + \mathbf{C}\dot{\mathbf{U}} + \mathbf{K}\mathbf{U} = \mathbf{F}, \tag{3.1}$$

where

$$\mathbf{M} = \begin{bmatrix} M_{\psi_\Gamma\psi_\Gamma} & M_{\psi_\Gamma\psi_{\Omega_f}} & 0 \\ M_{\psi_{\Omega_f}\psi_\Gamma} & M_{\psi_{\Omega_f}\psi_{\Omega_f}} & M_{\psi_{\Omega_f}\psi_{\Gamma_a}} \\ 0 & M_{\psi_{\Gamma_a}\psi_{\Omega_f}} & M_{\psi_{\Gamma_a}\psi_{\Gamma_a}} \end{bmatrix}, \tag{3.2}$$

$$\mathbf{C} = \begin{bmatrix} 0 & 0 & 0 \\ 0 & 0 & 0 \\ 0 & 0 & C^a \end{bmatrix}, \tag{3.3}$$

$$\mathbf{K} = \begin{bmatrix} K_{\psi_\Gamma\psi_\Gamma} & K_{\psi_\Gamma\psi_{\Omega_f}} & 0 \\ K_{\psi_{\Omega_f}\psi_\Gamma} & K_{\psi_{\Omega_f}\psi_{\Omega_f}} & K_{\psi_{\Omega_f}\psi_{\Gamma_a}} \\ 0 & K_{\psi_{\Gamma_a}\psi_{\Omega_f}} & K_{\psi_{\Gamma_a}\psi_{\Gamma_a}} + K^a \end{bmatrix}. \tag{3.4}$$

U is the vector of the unknown nodal quantities, i.e.

$$\mathbf{U}^T = [\psi_\Gamma^T,\ \psi_{\Omega_f}^T,\ \bar{\psi}_{\Gamma_a}^T], \tag{3.5}$$

and

$$\mathbf{F}^T = [\mathbf{f}_{\psi_\Gamma}^T,\ 0^T,\ 0^T]. \tag{3.6}$$

In the above, $\bar{\psi}_{\Gamma_a}^T = \left[\psi_{\Gamma_a}^T,\ \mathbf{q}_{\Gamma_a}^{(1)^T},\ \mathbf{q}_{\Gamma_a}^{(2)^T}\right]$, $\mathbf{f}_{\psi_\Gamma}$ is the discretized form of the right-hand side of (2.17), and ψ_Γ, ψ_{Ω_f} and ψ_{Γ_a} denote partitions of ψ over Γ, $\hat{\Omega}_f$ and $\hat{\Gamma}_a$, respectively.

The subscripts in the matrices and vectors (3.2)–(3.6) are used in order to identify the parts of the domain and the particular variable that contribute to the individual matrices. The matrices **M** (3.2) and **K** (3.4) consist of two sets of block-diagonal matrices; the top left blocks are the standard mass and stiffness matrices associated with the fluid; the bottom right blocks in **C** (3.3) and in **K** (3.4) represent the effective damping and stiffness of the absorbing boundary. Notice that the only coupling in the mass and stiffness matrices occurs between the fluid and the absorbing boundary; indeed only through the stiffness matrix. The only damping in the actual, unbounded, system comes from the radiated energy, which, in our formulation, is modeled through the bottom right block of **C** associated with the absorbing boundary.

3.2. *Absorbing boundary elements*

From (3.2)–(3.4), it is seen that the absorbing boundary is completely characterized by the damping and stiffness matrices C^a and K^a, defined by

$$C^a = \begin{bmatrix} C^a_{\psi_{\Gamma_a}\psi_{\Gamma_a}} & 0 & 0 \\ 0 & C^a_{q^{(1)}_{\Gamma_a} q^{(1)}_{\Gamma_a}} & 0 \\ 0 & 0 & C^a_{q^{(2)}_{\Gamma_a} q^{(2)}_{\Gamma_a}} \end{bmatrix}, \tag{3.7}$$

$$K^a = \begin{bmatrix} K^a_{\psi_{\Gamma_a}\psi_{\Gamma_a}} & K^a_{\psi_{\Gamma_a} q^{(1)}_{\Gamma_a}} & K^a_{\psi_{\Gamma_a} q^{(2)}_{\Gamma_a}} \\ K^a_{q^{(1)}_{\Gamma_a}\psi_{\Gamma_a}} & K^a_{q^{(1)}_{\Gamma_a} q^{(1)}_{\Gamma_a}} & 0 \\ K^a_{q^{(2)}_{\Gamma_a}\psi_{\Gamma_a}} & 0 & K^a_{q^{(2)}_{\Gamma_a} q^{(2)}_{\Gamma_a}} \end{bmatrix}. \tag{3.8}$$

Since C^a and K^a are local and symmetric, they can be constructed element by element and incorporated into the equations of motion by standard assembly techniques using existing finite element software. All that is necessary is to incorporate the element matrices c^a and k^a corresponding to the global C^a and K^a into the finite element library of an existing

software package for interior problems. The element matrices are given as[38,40]

$$\mathbf{k}^a = \frac{c}{2\gamma}\begin{bmatrix} \frac{2\gamma}{c}\mathbf{k}_{11} & \mathbf{k}_{12} & -\mathbf{k}_{13} \\ \mathbf{k}_{12}^T & -\mathbf{k}_{22} & 0 \\ -\mathbf{k}_{13}^T & 0 & \mathbf{k}_{33} \end{bmatrix}, \tag{3.9}$$

$$\mathbf{c}^a = \frac{c}{2\gamma^2}\begin{bmatrix} \frac{2\gamma^2}{c^2}\mathbf{c}_{11} & 0 & 0 \\ 0 & -\mathbf{c}_{22} & 0 \\ 0 & 0 & \mathbf{c}_{33} \end{bmatrix}, \tag{3.10}$$

with the following definitions for the individual matrices in (3.9)–(3.10):

$$\mathbf{k}_{11} = -\int_{\Gamma_a^e} H\mathbf{N}^e\mathbf{N}^{eT}d\Gamma_a^e, \tag{3.11}$$

$$\mathbf{k}_{22} = \int_{\Gamma_a^e} \overline{\nabla}^s\mathbf{N}^e \cdot \overline{\nabla}^s\mathbf{N}^{eT}d\Gamma_a^e, \tag{3.12}$$

$$\mathbf{k}_{33} = \int_{\Gamma_a^e} (H^2 - K)\mathbf{N}^e\mathbf{N}^{eT}d\Gamma_a^e, \tag{3.13}$$

$$\mathbf{k}_{12} = \int_{\Gamma_a^e} \overline{\nabla}^s\mathbf{N}^e \cdot \overline{\nabla}^s\mathbf{N}^{eT}d\Gamma_a^e, \tag{3.14}$$

$$\mathbf{k}_{13} = \int_{\Gamma_a^e} (H^2 - K)\mathbf{N}^e\mathbf{N}^{eT}d\Gamma_a^e, \tag{3.15}$$

$$\mathbf{c}_{11} = \int_{\Gamma_a^e} \mathbf{N}^e\mathbf{N}^{eT}d\Gamma_a^e, \tag{3.16}$$

$$\mathbf{c}_{22} = \mathbf{k}_{22}, \tag{3.17}$$

$$\mathbf{c}_{33} = \mathbf{k}_{33}. \tag{3.18}$$

In the above, $d\Gamma_a^e$ and the operator $\overline{\nabla}^s$ denote the area differential and the approximation of the surface gradient ∇^s on an element Γ_a^e of Γ_a, respectively. $\mathbf{N}^e$ denotes the usual element approximations, e.g. linear isoparametric approximations.

The element matrices (3.9)–(3.10) essentially give rise to a new absorbing boundary element — transient or time-harmonic — which is capable of approximately absorbing the waves that reach the artificial boundary while simulating the effect of the truncated infinite domain. Notice that the new absorbing element is a surface-only element (Fig. 5). One need only mesh the finite region $\hat{\Omega}_f$ and simply attach the absorbing element on the boundary $\hat{\Gamma}_a$ without any further discretization within the semi-infinite exterior region. Standard quadrature rules can be used to evaluate the entries in the element matrices.

We remark that while the discussion here has been limited to scattering problems pertaining to a rigid structure, the modifications needed to accommodate radiation problems and/or penetrable scatterers are straightforward (e.g. see Ref. 41).

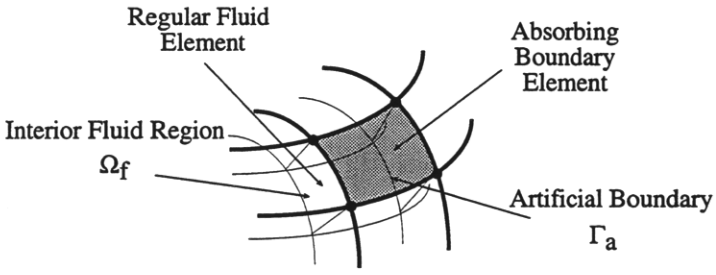

Fig. 5. Typical geometry of absorbing transient/time-harmonic boundary element.

4. The Exact Problem

In order to validate the methodology outlined thus far, we sought to compare our numerical results with existing analytical solutions. Gaunaurd and Huang[42] have recently provided a series solution for the scattering problem of a spherical rigid scatterer near a plane boundary when insonified by a plane wave. The geometry of the problem is depicted in Fig. 6.

The authors in Ref. 42 obtained the total and scattered wavefields by using the method of images in conjunction with an addition theorem for spherical wave functions. The addition theorem used exhibits two distinct branches, one valid for the near-field, i.e. for radial distances less than that between the centers of the real and image scatterer (d in Fig. 6), and one valid outside this region. Herein, we repeat, as per Ref. 42, the expressions we used in order to calculate the analytical solution. To this end, we consider a traveling plane wave of the form:

$$\psi_{\text{inc}}(x,\, y,\, z,\, t) = e^{ik(x\cos\alpha_x + y\cos\alpha_y + z\cos\alpha_z)} e^{-i\omega t}\,, \tag{4.1}$$

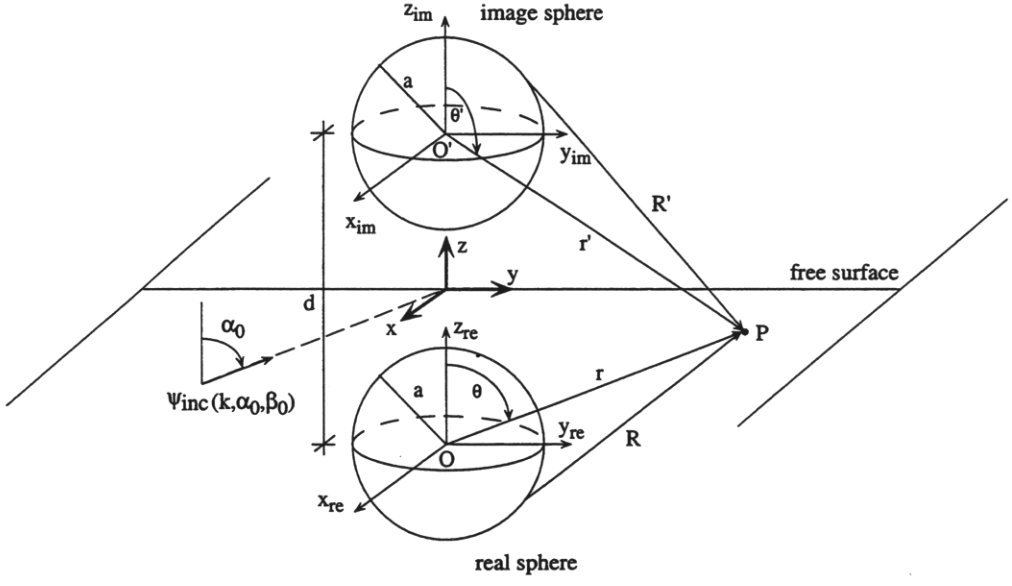

Fig. 6. Geometry of a rigid spherical scatterer in a half-space; real and image spheres.

where α_x, α_y, and α_z are the angles formed between the normal to the plane of the traveling front and the three coordinate axes (x, y, z); ω denotes frequency; $k = \omega/c$ is the wavenumber; and i is the imaginary unit. Using spherical coordinates (r, θ, ϕ) for the system that has origin at O (Fig. 6), (4.1) can be rewritten as

$$\psi_{\text{inc}}(r, \theta, \phi) = e^{ikr(\cos(\phi-\beta_0)\sin\theta\sin\alpha_0+\cos\theta\cos\alpha_0)}e^{-ik\frac{d}{2}\cos\alpha_0}$$

$$= 4\pi e^{-ik\frac{d}{2}\cos\alpha_0}\sum_{q=0}^{\infty} i^q j_q(kr)\sum_{p=-q}^{p=q} Y^*_{qp}(\alpha_0, \beta_0)Y_{qp}(\theta, \phi)\,. \tag{4.2}$$

r is the radial distance and θ, ϕ denote the polar and meridional angles, respectively; j_q is the spherical Bessel function; (k, α_0, β_0) is the incident wavevector and an asterisk $(^*)$ denotes complex conjugate. In deriving (4.2), use was made of a spherical representation for plane waves[43] and of the following relations that connect the propagation angles in the cartesian and spherical systems:

$$\cos\alpha_x = \cos\beta_0\sin\alpha_0\,, \tag{4.3}$$

$$\cos\alpha_y = \sin\beta_0\sin\alpha_0\,, \tag{4.4}$$

$$\cos\alpha_z = \cos\alpha_0\,. \tag{4.5}$$

In Ref. 42, three additional wavefields are defined, namely, the one reflected from the free surface (ψ_{refl}), the scattered one due to the real sphere ($\psi^{\text{sph}}_{\text{sc}}$) (if it alone was occupying the full-space and was insonified by ψ_{inc}), and the scattered field due to the image sphere ($\psi^{\text{ima}}_{\text{sc}}$) (again if the image sphere alone was occupying the full-space and was insonified by ψ_{refl}). The sum of all four fields is equal to the total pressure field for the half-space problem, i.e.

$$\psi_{\text{tot}} = \psi_{\text{inc}} + \psi_{\text{refl}} + \psi = \psi_{\text{inc}} + \psi_{\text{refl}} + \psi^{\text{sph}}_{\text{sc}} + \psi^{\text{ima}}_{\text{sc}}\,, \tag{4.6}$$

where

$$\psi_{\text{refl}}(r, \theta, \phi) = -e^{ikr(\cos(\phi-\beta_0)\sin\theta\sin\alpha_0-\cos\theta\cos\alpha_0)}e^{ik\frac{d}{2}\cos\alpha_0}$$

$$= -4\pi e^{ikd\cos\alpha_0}\sum_{q=0}^{\infty} i^q j_q(kr)\sum_{p=-q}^{p=q}(-1)^{q+p}Y^*_{qp}(\alpha_0, \beta_0)Y_{qp}(\theta, \phi)\,, \tag{4.7}$$

$$\psi^{\text{sph}}_{\text{sc}}(r, \theta, \phi) = 4\pi\sum_{q=0}^{\infty}\sum_{p=-q}^{p=q} b_{qp}h^{(1)}_q(kr)Y_{qp}(\theta, \phi)\,, \tag{4.8}$$

$$\psi^{\text{ima}}_{\text{sc}}(r', \theta', \phi') = -4\pi\sum_{q=0}^{\infty}\sum_{p=-q}^{p=q}(-1)^{q+p}b_{qp}h^{(1)}_q(kr')Y_{qp}(\theta', \phi')\,. \tag{4.9}$$

(r, θ, ϕ) and (r', θ', ϕ') are the coordinate systems with centers at O and O' as per Fig. 6; $h^{(1)}_q$ is the spherical Hankel function of the first kind (a time factor of $e^{-i\omega t}$ has been assumed throughout) and $Y_{qp}(\theta, \phi)$ is a spherical harmonic that is given as[43]:

$$Y_{qp}(\theta, \phi) = \sqrt{\frac{(2q+1)}{4\pi}\frac{(q-p)!}{(q+p)!}}P^p_q(\cos\theta)e^{ip\phi}\,. \tag{4.10}$$

It can be easily verified that ψ_{tot} in (4.6) satisfies the pressure-free boundary condition on the free surface ($\psi_{\text{tot}} = 0$). To satisfy the zero Neumann condition ($\partial\psi_{\text{tot}}/\partial r = 0$) on the surface of the real scatterer, the authors in Ref. 42 used an addition theorem for spherical wave functions[44] in order to express (4.9) in the unprimed system (Fig. 6). The resulting form for the total pressure is:

$$\psi_{\text{tot}}(r, \theta, \phi) = 4\pi \sum_{q=0}^{\infty} \sum_{p=-q}^{p=q} \left[i^q j_q(kr) Y_{qp}^*(\alpha_0, \beta_0) \left[e^{-ik\frac{d}{2}\cos\alpha_0} - (-1)^{q+p} e^{ik\frac{d}{2}\cos\alpha_0} \right] \right.$$
$$\left. + b_{qp} h_q^{(1)}(kr) - \sum_{n=|p|}^{\infty} (-1)^{n+p} b_{np} Q_{pnpq}(d) \begin{Bmatrix} j_q(kr), & r \le d \\ h_q^{(1)}(kr), & r > d \end{Bmatrix} \right] Y_{qp}(\theta, \phi) . \tag{4.11}$$

where

$$Q_{pqpn}(d) = \sqrt{(2n+1)(2q+1)}\, i^{-q+n} (-1)^p$$
$$\times \sum_{\sigma=|q-n|}^{q+n} (-1)^\sigma i^\sigma (2\sigma+1) \begin{pmatrix} q & n & \sigma \\ 0 & 0 & 0 \end{pmatrix} \begin{pmatrix} q & n & \sigma \\ p & -p & 0 \end{pmatrix} \begin{Bmatrix} h_\sigma^{(1)}(kd), & r \le d \\ j_\sigma(kd), & r > d \end{Bmatrix} . \tag{4.12}$$

In the above, the terms in large parentheses in the series of (4.12) denote Wigner 3-j symbols.[45]

Next, using the Neumann condition on the real scatterer, it is possible to proceed in the way described in Ref. 42 in order to obtain an infinite system of algebraic equations for the determination of the unknown coefficients b_{qp} involved in the series (4.11).

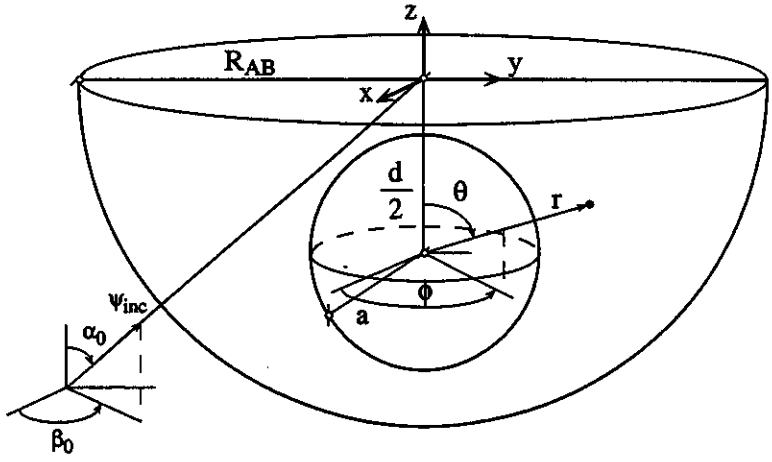

Fig. 7. Model geometry of a rigid, spherical scatterer in a half-space with a surrounding semi-spherical artificial boundary.

5. Numerical Results

We consider a rigid spherical scatterer submerged in a half-space at two different depths of immersion, namely at $d/a = 2$ and $d/a = 3$ (Fig. 7). The scatterer is insonified by a traveling plane wave ψ_{inc}; in this paper, we consider only time-harmonic response.

Results are obtained by using both the absorbing boundary elements described in Sec. 3 and the analytical solutions described in Sec. 4. We compare the two sets for a small

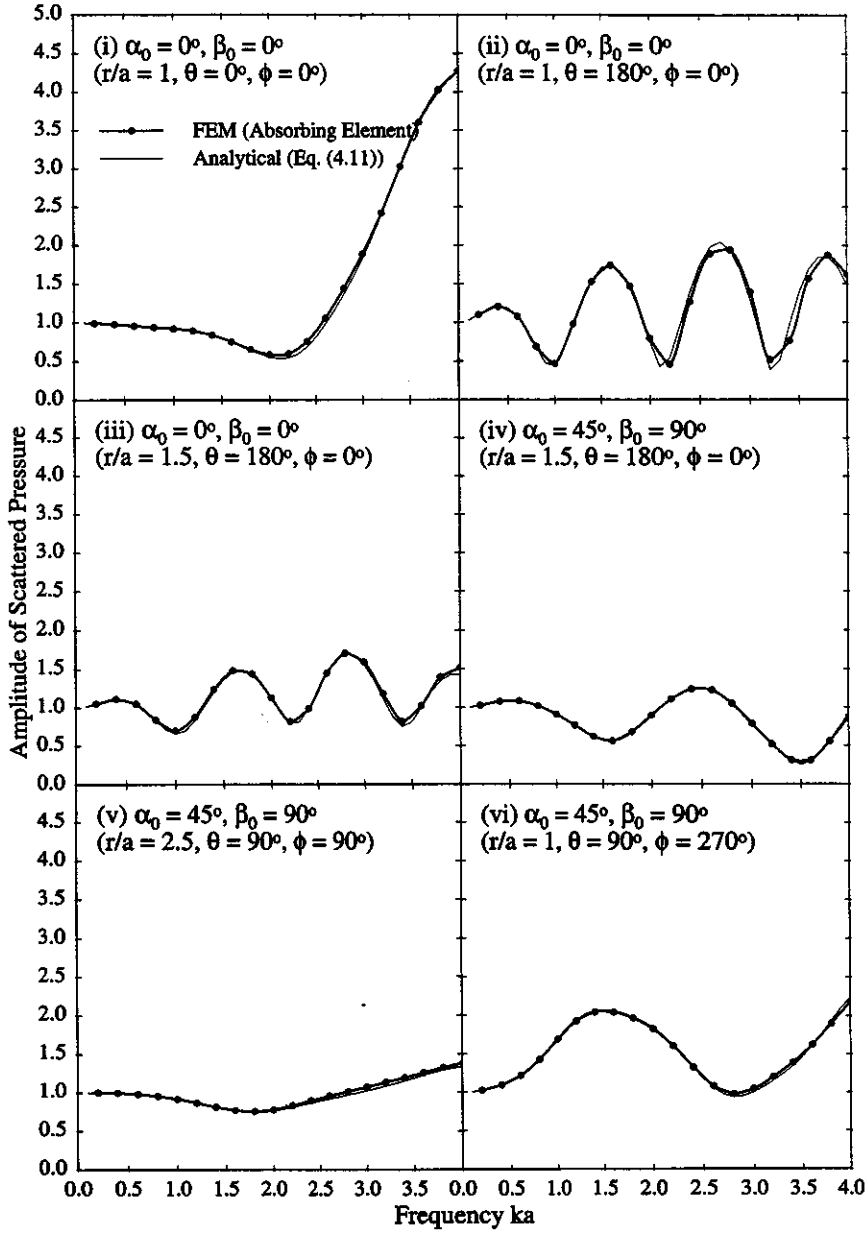

Fig. 8. Scattered pressure amplitude; depth of immersion $d/a = 3$; artificial boundary radius $R_{AB}/a = 3$.

frequency range ($ka = 0$ to 4) in order to assess the performance of the numerical method. In all cases where absorbing elements were used, those were described on a semi-spherical artificial boundary of radius R_{AB}. With this particular choice of geometry for the artificial boundary, the term $H^2 - K$ in (3.13), (3.15) and (3.18) vanishes identically. Consequently, with our particular choice of isoparametric approximations for the shape functions $\mathbf{N}^e$, the

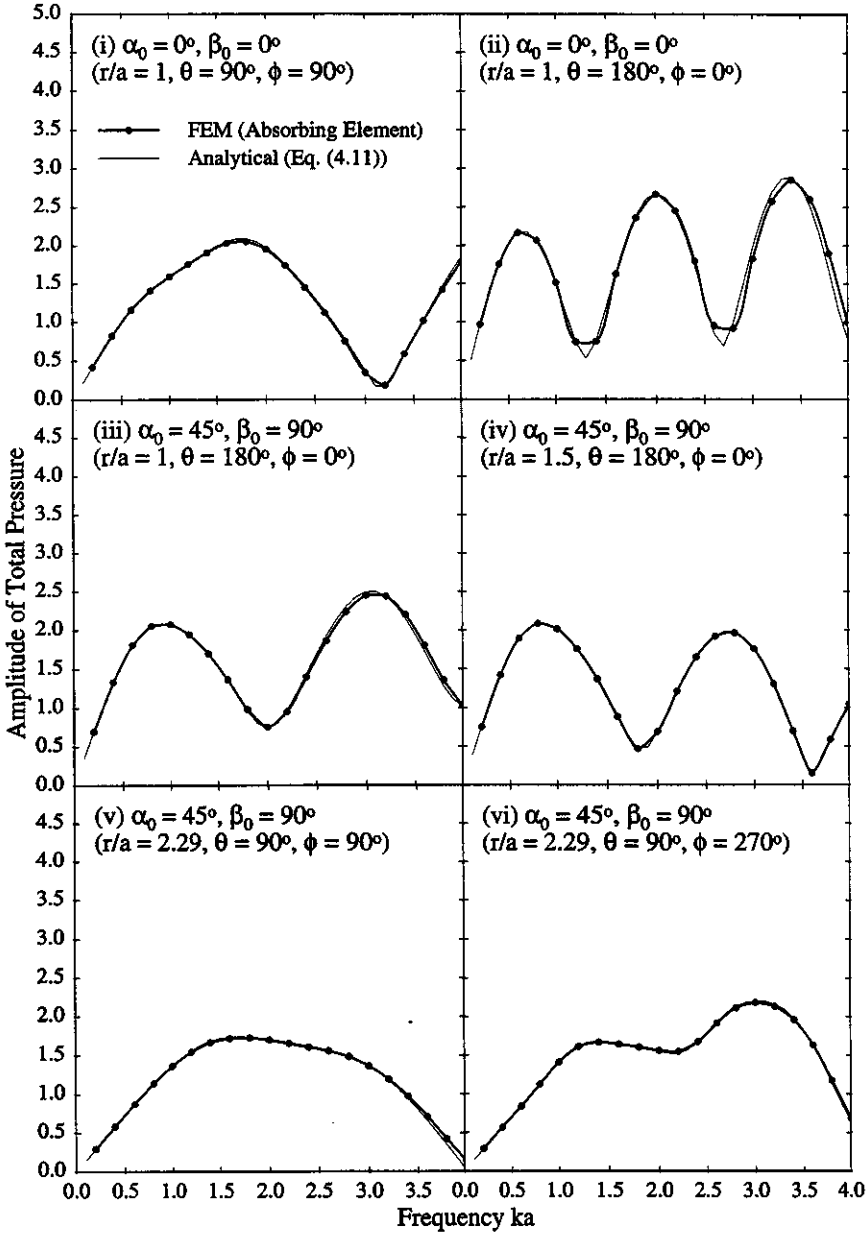

Fig. 9. Total pressure amplitude; depth of immersion $d/a = 2$; artificial boundary radius $R_{AB}/a = 2.5$.

resulting absorbing element stiffness and damping matrices are only 8×8, as there are only two degrees of freedom per surface node on the boundary — one for the pressure ψ and one for the auxiliary variable $q^{(1)}$. Furthermore, in all cases, we used $\gamma = R_{AB}/c$; for this particular value of the stability parameter and for a spherical artificial boundary, it can be shown[38,40] that the second-order condition (2.8) is identical to one derived by Bayliss and Turkel.[21] While we have not yet tried other artificial boundary shapes, e.g. an ellipsoid, such boundaries can be obtained directly by using the present formulation and applied in cases of highly elongated scatterers.

For the excitation, we considered two cases of incidence, namely at ($\alpha_0 = 0°$, $\beta_0 = 0°$) and ($\alpha_0 = 45°$, $\beta_0 = 90°$). The radius of the artificial boundary was chosen to be $R_{AB}/a = 3$ when $d/a = 3$, and $R_{AB}/a = 2.5$ when $d/a = 2$. The implication of these choices is that for the highest frequency considered in our examples ($ka = 4$), the absorbing boundary is placed as close to the scatterer as one third of the shortest acoustic wavelength ($\pi/2$). We used linear tetrahedra for meshing the fluid region and linear triangles as the absorbing elements on the artificial boundary (naturally, only the half-space region needs to be meshed). In order for our mesh to resolve the shortest wavelengths accurately, the resulting discretization comprised 45,996 linear tetrahedra and 2,592 absorbing elements for an immersion depth of $d/a = 2$; the total number of degrees of freedom was 9,546.

We used (4.11) to obtain analytic solutions. Usually, 15 to 20 terms were sufficient for convergence of the series in (4.11) (the relative tolerance used was 10^{-6}).

Figures 8 and 9 depict scattered and total pressure amplitudes for both analytic and finite element solutions at various points, depths of immersion, and angles of incidence. As can be seen, there is close agreement between the two sets in all cases.

6. Concluding Remarks

The primary objective of this paper was to illustrate the application of recently developed absorbing boundary elements to half-space problems. We provided the theoretical foundation for the use, in half-space problems, of a second-order absorbing boundary condition and its associated absorbing element, developed originally for a full-space. We provided illustrative results using the absorbing elements for a rigid spherical scatterer in the frequency-domain and compared them against an exact solution. The attractiveness of the new elements presented here lies in the fact that they can be used in either transient or harmonic steady-state problems with conventional finite elements while placed at a small distance from the scatterer — only a fraction of the dominant acoustic wavelength.

References

1. A. Sommerfeld, *Partial Differential Equations in Physics* (Academic Press, New York, 1949).
2. D. Givoli, "Non-reflecting boundary conditions: A review," *J. Comput. Phys.* **94**(1) (1991), 1–29.
3. D. Givoli, *Numerical Methods for Problems in Infinite Domains* (Elsevier Science Publishers, Amsterdam, 1992).
4. P. Bettess and J. A. Bettess, "Infinite elements for dynamic problems: Part 1," *Eng. Comput.* **8** (1991), 99–124.

5. P. Bettess and J. A. Bettess, "Infinite elements for dynamic problems: Part 2," *Eng. Comput.* **8** (1991), 125–151.
6. P. Bettess, *Infinite Elements* (Penshaw Press, Sunderland, 1992).
7. I. Harari and T. J. R. Hughes, "A cost comparison of boundary element and finite element methods for problems of time-harmonic acoustics," *Comput. Methods Appl. Mech. Eng.* **97** (1992), 77–102.
8. X. Zeng, L. F. Kallivokas and J. Bielak, "Stable localized symmetric integral equation method for acoustic scattering problems," *J. Acoust. Soc. Am.* **91**(5) (1992), 2510–2518.
9. X. Zeng and J. Bielak, "Exterior stable domain segmentation integral equation method for scattering problems," *Int. J. Num. Meth. Eng.* **37** (1994), 777–792.
10. W. J. Mansur and C. A. Brebbia, "Formulation of the boundary element method for transient problems governed by the scalar wave equation," *Appl. Math. Modelling* **6** (1982), 307–311.
11. W. J. Mansur and C. A. Brebbia, "Numerical implementation of the boundary element method for two dimensional transient scalar wave propagation problems," *Appl. Math. Modelling* **6** (1982), 299–306.
12. A. S. M. Israil and P. K. Banerjee, "Advanced development of time-domain BEM for two-dimensional scalar wave propagation," *Int. J. Num. Meth. Eng.* **29** (1990), 1003–1020.
13. A. S. M. Israil and P. K. Banerjee, "Two-dimensional transient wave-propagation problems by time-domain BEM," *Int. J. Solids Struct.* **26**(8) (1990), 851–864.
14. R. C. MacCamy and S. P. Marin, "A finite element method for exterior interface problems," *Int. J. Math. Sci.* **3** (1980), 311–350.
15. D. Givoli and J. B. Keller, "A finite element method for large domains," *Comput. Methods Appl. Mech. Eng.* **76** (1989), 41–66.
16. D. Givoli and J. B. Keller, "Non-reflecting boundary conditions for elastic waves," *Wave Motion* **12** (1990), 261–279.
17. I. Harari and T. J. R. Hughes, "Galerkin/least-squares finite element methods for the reduced wave equation with non-reflecting boundary conditions in unbounded domains," *Comput. Methods Appl. Mech. Eng.* **98** (1992), 411–454.
18. D. Givoli, "A spatially exact non-reflecting boundary condition for time-dependent problems," *Comput. Methods Appl. Mech. Eng.* **95** (1992), 97–113.
19. B. Engquist and A. Majda, "Absorbing boundary conditions for the numerical simulation of waves," *Math. Comp.* **31** (1977), 629–651.
20. B. Engquist and A. Majda, "Radiation boundary conditions for acoustic and elastic wave calculations," *Comm. Pure Appl. Math.* **32** (1979), 313–357.
21. A. Bayliss and E. Turkel, "Radiation boundary conditions for wave-like equations," *Comm. Pure Appl. Math.* **33** (1980), 707–725.
22. A. Bayliss and E. Turkel, "Far field boundary conditions for compressible flows," *J. Comp. Phys.* **48** (1982), 182–199.
23. A. Bayliss, M. Gunzburger and E. Turkel, "Boundary conditions for the numerical solution of elliptic equations in exterior regions," *SIAM J. Appl. Math.* **42**(2) (1982), 430–451.
24. J. Assaad, J.-N. Decarpigny, C. Bruneel, R. Bossut and B. Hamonic, "Application of the finite element method to two-dimensional radiation problems," *J. Acoust. Soc. Am.* **94**(1) (1993), 562–573.
25. P. M. Pinsky and N. N. Abboud, "Transient finite element analysis of the exterior structural acoustics problem," ASME *J. Vib. Acoust.* **112** (1990), 245–256.
26. P. M. Pinsky and N. N. Abboud, "Finite element solution of the transient exterior structural acoustics problem based on the use of radially asymptotic boundary operators," *Comput. Methods Appl. Mech. Eng.* **85** (1991), 311–348.
27. P. M. Pinsky, L. L. Thompson and N. N. Abboud, "Local high-order radiation boundary

conditions for the two-dimensional time-dependent structural acoustics problem," *J. Acoust. Soc. Am.* **91**(3) (1992), 1320–1335.
28. T. L. Geers, "Doubly asymptotic approximations for transient motions of submerged structures," *J. Acoust. Soc. Am.* **64**(5) (1978), 1500–1508.
29. T. L. Geers and C. A. Felippa, "Doubly asymptotic approximations for vibration analysis of submerged structures," *J. Acoust. Soc. Am.* **73**(4) (1983), 1152–1159.
30. D. Givoli and J. B. Keller, "Special finite elements for use with high-order boundary conditions," *Comput. Methods Appl. Mech. Eng.* **119** (1994), 199–213.
31. O. C. Zienkiewicz and P. Bettess, "Infinite elements in the study of fluid structure interaction problems," *Proc. 2nd Int. Symp. Comp. Methods Appl. Sci.*, Versailles, 1975.
32. O. C. Zienkiewicz, C. Emson and P. Bettess, "A novel boundary infinite element," *Int. J. Num. Meth. Eng.* **19** (1983), 393–404.
33. O. C. Zienkiewicz, K. Bando, P. Bettess, C. Emson and T. C. Chiam, "Mapped infinite elements for exterior wave problems," *Int. J. Num. Meth. Eng.* **21** (1985), 1229–1251.
34. D. S. Burnett, "A three-dimensional acoustic infinite element based on a prolate spheroidal multipole expansion," *J. Acoust. Soc. Am.* **96**(5) pt.1 (1994), 2798–2816.
35. R. J. Astley, G. J. Macaulay and J. P. Coyette "Mapped wave envelope elements for acoustical radiation and scattering," *J. Sound Vib.* **170**(1) (1994), 97–118.
36. R. J. Astley, "Transient wave envelope elements for wave problems," *J. Sound Vib.* **192**(1) (1996), 245–261.
37. L. F. Kallivokas and J. Bielak, "Time-domain analysis of transient structural acoustics problems based on the finite element method and a novel absorbing boundary element," *J. Acoust. Soc. Am.* **94**(6) (1993), 3480–3492.
38. L. F. Kallivokas, "Absorbing boundaries conditions and finite elements for transient and harmonic steady-state acoustic fluid-structure interaction," Ph.D. Thesis, Carnegie Mellon University, 1994.
39. L. F. Kallivokas and J. Bielak, "A time-domain impedance element for FEA of axisymmetric exterior structural acoustics," *ASME J. Vib. Acoust.* **117** (1995), 145–151.
40. L. F. Kallivokas, J. Bielak and R. C. MacCamy, "A simple impedance-infinite element for the finite element solution of the three-dimensional wave equation in unbounded domains," *Comput. Methods Appl. Mech. Eng.* (submitted).
41. L. F. Kallivokas and J. Bielak, "Transient and time-harmonic infinite elements for near-surface computations of three-dimensional structures submerged in a half-space," *Symposium on Acoustics of Submerged Structures & Transduction Systems, ASME 15th Biennial Conference on Mechanical Vibration and Noise*, Boston, MA, 1995.
42. G. C. Gaunaurd and H. Huang, "Acoustic scattering by a spherical body near a plane boundary," *J. Acoust. Soc. Am.* **96**(4) (1994), 2526–2536.
43. J. D. Jackson, *Classical Electrodynamics* (John Wiley & Sons, New York, 1975).
44. S. Stein, "Addition theorems for spherical wave functions," *Quart. Appl. Math.* **19** (1961), 15–24.
45. M. Rotenberg, R. Bivins, N. Metropolis and J. K. Wooten. Jr, *The 3-j and 6-j symbols* (Cambridge Technology Press, MIT, 1959).